IUPAC Technical Report

Clive Bucknall*, Volker Altstädt, Dietmar Auhl, Paul Buckley, Dirk Dijkstra, Andrzej Galeski, Christoph Gögelein, Ulrich A. Handge, Jiasong He, Chen-Yang Liu, Goerg Michler, Ewa Piorkowska, Miroslav Slouf, Iakovos Vittorias and Jun Jie Wu

Structure, processing and performance of ultra-high molecular weight polyethylene (IUPAC Technical Report). Part 3: deformation, wear and fracture

https://doi.org/10.1515/pac-2019-0406
Received April 6, 2019; accepted March 23, 2020

Abstract: Three grades of polyethylene, with weight-average relative molar masses, $\overline{M}_W$, of approximately 0.6×10^6, 5×10^6, and 9×10^6, were supplied as compression mouldings by a leading manufacturer of ultra-high molecular weight polyethylene (UHMWPE). They were code-named PE06, PE5, and PE9, respectively. Specimens cut from these mouldings were subjected to a wide range of mechanical tests at 23 °C. In tensile tests, deformation was initially elastic and dominated by crystallinity, which was highest in PE06. Beyond the yield point, entanglement density became the dominant factor, and at 40 % strain, the rising stress–strain curves for PE5 and PE9 crossed the falling PE06 curve. Fracture occurred at strains above 150 %. Differences in stress–strain behaviour between PE5 and PE9 were relatively small. A similar pattern of behaviour was observed in wear tests; wear resistance showed a marked increase when $\overline{M}_W$ was raised from 0.6×10^6 to 5×10^6, but there was no further increase when it was raised to 9×10^6. It is concluded that the unexpected similarity in behaviour between PE5 and PE9 was due to incomplete consolidation during moulding, which led to deficiencies in entanglement at grain boundaries; they were clearly visible on the surfaces of both tensile and wear specimens. Fatigue crack growth in 10 mm thick specimens was so severely affected by inadequate consolidation that it forms the basis for a separate report – Part 4 in this series.

Keywords: consolidation; fatigue; fracture; IUPAC Polymer Division; UHMWPE; wear; yielding.

Article note: Sponsoring body: IUPAC Polymer Division: see more details on page 1518.

***Corresponding author: Clive Bucknall**, School of Aerospace, Transport & Manufacturing B 61, Cranfield University, Bedford, MK43 0AL, UK, e-mail: clivebucknall@aol.com
Volker Altstädt: Department of Polymer Engineering, Universität Bayreuth, Bayreuth, Germany
Dietmar Auhl: Fakultät III – Werkstoffwissenschaft Technische, Universität Berlin, Berlin, D-10623, Germany
Paul Buckley: Department of Engineering Science, University of Oxford, Oxford, OX1 3PJ, UK
Dirk Dijkstra: Covestro Deutschland AG, Leverkusen, Germany
Andrzej Galeski and Ewa Piorkowska: Centre for Molecular and Macromolecular Sciences, Polish Academy of Sciences, Lodz, Poland
Christoph Gögelein: Arlanxeo Deutschland GmbH, Dormagen, Germany
Ulrich A. Handge: Institute of Polymer Research, Helmholtz-Zentrum Geesthacht, Max-Planck-Strasse 1, 21502, Geesthacht, Germany
Jiasong He and Chen-Yang Liu: Chinese Academy of Sciences, Laboratory of Polymer Science and Materials, Beijing, China, 100190
Goerg Michler: Martin-Luther-Universität, Halle-Wittenberg, Germany
Miroslav Slouf: Institute of Macromolecular Chemistry CAS, Prague, Czech Republic
Iakovos Vittorias: Omya International AG, Baslerstrasse 42, CH-4665, Oftringen, Switzerland
Jun Jie Wu: Department of Engineering, Durham University, Stockton Road, Durham, DH1 3LE, UK

CONTENTS

1 Introduction

The polymer industry employs a wide range of tests to ensure that thermoplastics perform well in load-bearing applications. They range from characterising relative molar mass distributions using size exclusion chromatography (SEC), through modelling of melt flow during processing, to trials of the finished product under service conditions. For most applications, this approach has proved highly successful. Once a satisfactory method of manufacture has been developed, quality control (QC) and quality assurance (QA) tests can be used routinely to maintain standards at a high level. Unfortunately, applying that approach to ultra-high molecular weight polyethylene (UHMWPE) presents a number of problems.

In response to these problems, the authors of this report formed an IUPAC Task Group to carry out a comprehensive program of standard and non-standard testing. Part 1 in this series examines the limitations of available methods for characterizing weight-average molar mass, $\overline{M}_W$, molar mass distribution, and the rheological properties of UHMWPE above its melting point. Part 2 deals with the use of microscopy and other techniques to study crystal structure, crystallization, crystallinity, super-molecular structure, and thermally induced transitions.

The present report is concerned broadly with mechanical properties, and particularly with the ability of available test methods to detect and characterise structural defects in compression-moulded UHMWPE specimens. The most demanding applications of this family of polymers are in total joint replacements, which inevitably lose some material through wear. Unfortunately, in a significant minority of cases, polyethylene wear debris particles with diameters between 0.1 and 1.0 μm initiate adverse immune reactions, resulting in painful arthritis, bone loss, and loosening of the implant, so that replacement surgery becomes necessary. Currently, standard pin-on-disc wear tests simply measure rates of weight loss, not particle size, and most of the available data on the dimensions of wear debris particles, especially those generated by hip and knee prostheses, comes from the operating theatre. Simulation testing of wear behaviour is expensive and time-consuming, but can provide essential information about the factors controlling distributions of particle sizes in wear debris.

2 Results

2.1 Materials

Three large batches of polyethylene, with weight average relative molar masses of about 0.6×10^6, 5×10^6, and 9×10^6 were supplied by a major manufacturer of UHMWPE. The batches are identified in this report by the

codenames PE06, PE5, and PE9, respectively. For convenience, the term UHMWPE is applied to all three materials, although PE06 should strictly be classified as HMWPE, because its $\overline{M}_W$ is below 10^6. Except for one set of plaques moulded at Oxford University (see Section 2.2 below), all mechanical tests were carried out on compression mouldings made by the polymer manufacturer purely from as-polymerized reactor powder, without additives, as the company's contribution to the IUPAC project. Consequently, the materials tested during this study do not necessarily have the same properties as commercial grades of UHMWPE.

2.2 Standard tensile testing

Three laboratories carried out conventional uniaxial tensile tests at 23 °C, in accordance with ASTM and ISO standards [1, 2]. Following standard practice, most of the resulting data are expressed in this section in terms of nominal stress, $\sigma (= F/A_0)$, and nominal strain, $\varepsilon (= \Delta L/L_0)$, where F is the applied tensile force, A_0 is the initial cross-sectional area, and L_0 is the initial gauge length. However, in some cases it is more convenient to discuss relationships between true stress, σ_t, and true strain, ε_t, which are defined as follows:

$$\sigma_t = \sigma(1 + \varepsilon) \tag{1}$$

$$\varepsilon_t = \ln(1 + \varepsilon) \tag{2}$$

Results from one set of tensile tests are presented in Fig. 1 and in Table 1, where the combined standard uncertainty, u_c, for yield stress is ±2 %. They show that PE06 has the highest yield stress and the largest elongation at break. There are only small differences between the stress–strain curves of the two UHMWPE grades. Both have relatively low yield stresses, but subsequently strain-harden quite rapidly before breaking at an elongation of about 250 %.

Handge also measured secant modulus E at 23 °C, over the strain interval 0.05 to 0.25 %, at a strain rate of 3.3×10^{-4} s^{-1}. The resulting values of E were 1020 MPa for PE06, 624 MPa for PE5, and 610 MPa for PE9, with u_c = ±1.5 %.

Instead of testing mouldings made by the UHMWPE manufacturer, Buckley (OU) carried out a separate program of work to investigate the effects of molecular weight and consolidation temperature on mechanical properties by deliberately using below-optimum processing conditions to make some of the mouldings. Reactor powders from batches PE06, PE5, and PE9 were compression moulded at three dwell temperatures: 150, 165, and 180 °C, to produce sets of 3 mm thick sheets measuring 140 × 200 mm. The mould was heated

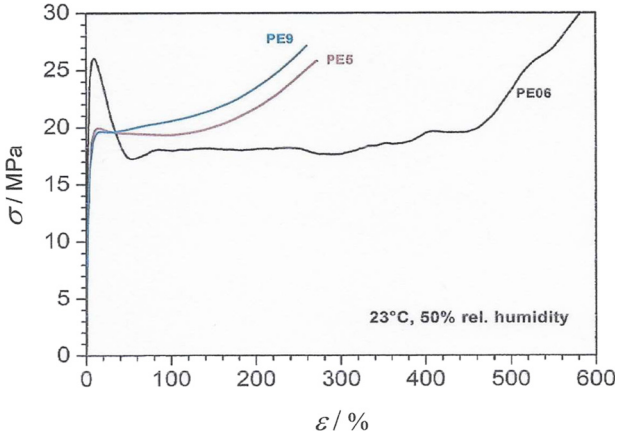

Fig. 1: Nominal stress–strain curves for PE06, PE5, and PE9. Nominal strain rate 0.833 mm/s. Data of Handge (HG).[1]

1 Laboratories contributing data for these reports are identified by a two-letter code – see Table 1 in Part 1.

Table 1: Tensile yield stress σ_y of compression-moulded UHMWPE materials; $u_c = \pm 2$ %.

Polymer	σ_y/MPa		
	PE06	PE5	PE9
Handge (HG)	25	20	20
Slouf (CZ)	26	20	20
Wu (DU)	25	19	19

gradually over about 30 min, with pressure applied when the temperature reached 145 °C. After reaching the selected dwell temperature, each melt was held at full pressure for 15 min; the mould was then cooled to 100 °C within 3 min. Previous compression moulding experiments at Oxford have shown poor consolidation of UHMWPE at temperatures below 150 °C, while raising the dwell temperature above 180 °C not only has little effect on consolidation, but also can cause significant oxidative degradation, leading to losses in both strength and ductility. A CNC milling machine was used without cutting lubricant to prepare dog-bone test specimens with 20 mm gauge length and 105 mm grip separation.

Tensile tests were carried out at 20 °C, in accordance with the ISO standard [2]. Results from these experiments are set out in Fig. 2 and Table 2. The one factor that clearly affects initial yielding is crystallinity. Both elastic modulus and yield stress are higher in PE06 than in PE5 or PE9, because both of these true UHMWPE grades exhibit retarded relaxation while they are cooling in the mould, as discussed in Part 2, so that crystallization is restricted. During subsequent stretching, drawing stresses in PE06 were not only lower than in PE5 and PE9, but they also showed less variation with moulding temperature. All three PE06 specimens extended to nominal strains of over 600 %. Tests were then terminated because grip separation in the Instron tensometer had reached its limit. At that point, the nominal strain was 198 % and nominal stresses were over 140 MPa. In PE5 and PE9, the curves for mouldings made at different temperatures began to diverge after reaching a nominal strain of 40 % and a nominal stress of 28 MPa. Coincidentally, the curves for all nine specimens meet at that same point on the loading curve. Fracture occurred at nominal strains between 140 and 155 %. The similarity in behaviour between PE5 and PE9 shows that raising $\overline{M}_W$ from 5×10^6 to 9×10^6 did not produce the expected effects of increased entanglement density in PE9. The simplest explanation for this result is that entanglement densities at 'grain' boundaries were lower than in the bulk of the moulding and made a disproportionate contribution to yielding and tensile drawing.

2.3 Cyclic tensile testing

Tensile specimens cut from plaques moulded at 150, 165, and 180 °C were subjected to cyclic loading at 20 °C, with a nominal strain rate $d\varepsilon/dt$ of 5×10^{-3} s^{-1}. Each specimen was first stretched under uniaxial tension to a

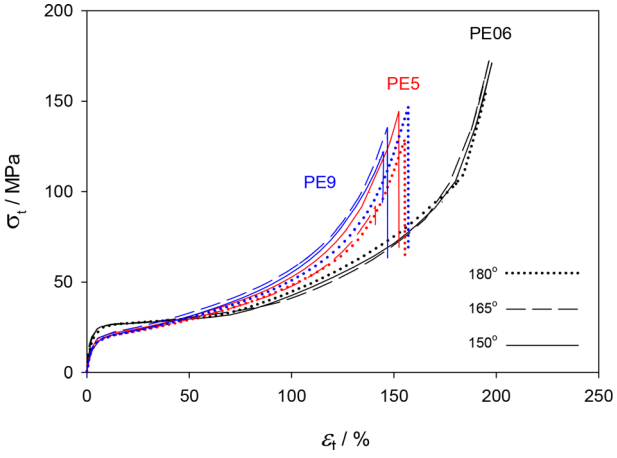

Fig. 2: Stress–strain curves for PE06, PE5, and PE9 at 20 °C, showing the effects of moulding temperature. Data from Buckley (OU). Laboratory record in which symbols σ_t and ε_t represent *tensile* stress and strain.

Table 2: Effects of moulding temperature on nominal tensile yield stress σ_y (MPa). Uncertainty $u_c = \pm 2$ %. Data from Buckley (OU).

Polymer				σ_y/MPa
	150 °C	165 °C	180 °C	Average
PE06	23.6	23.9	23.4	23.6
PE5	19.2	28.4	18.1	18.8
PE9	18.4	19.6	18.1	18.7

maximum nominal strain, ε_{max}, of 40 %. It was then subjected to five loading cycles between a tensile stress, σ, of zero and ε_{max} of 40 %. At the end of the fifth cycle, the maximum strain was raised to 60 % and the specimen was subjected to a further five cycles between zero stress and the new ε_{max}. For a final five cycles, ε_{max} was increased to 80 %. Results from these tests are presented in Fig. 3 as nominal stress–strain curves. All specimens produced large hysteresis loops. The effects of varying moulding temperature were found to be negligible and the differences between PE5 and PE9 were again small. As in the standard tensile tests, PE06 was distinguished by its high yield and drawing stresses during the early stages of each test.

To clarify the discussion of plastic deformation under cyclic loading, it is helpful to convert nominal stresses and strains into true stresses and true strains. A quantity of particular interest in the present context is the *relative residual true strain*, ε_r^*, which measures the residual strain in the specimen after unloading relative to the strain reached at peak load during that most recent cycle. It is defined as follows:

$$\varepsilon_r^* = \frac{\varepsilon_{t,r}}{\varepsilon_{t,max}} \tag{3}$$

where $\varepsilon_{t,max}$ is the maximum true strain at peak load for each cycle and $\varepsilon_{t,r}$ is the residual true strain after subsequent unloading. Table 3 shows that ε_r^* is unaffected by moulding temperature over the range 150–180 °C but increases with maximum true strain. Residual strains were higher in PE06 than in PE5 and PE9, indicating that plastic flow processes played a greater part in the deformation of PE06 than they did in PE5 or PE9, where the exceptionally long chains of these polymers hindered relaxation and promoted elastic behaviour.

In cyclic loading tests, the specific hysteresis energy ΔW is defined as the energy dissipated **per unit volume** during a single cycle, and the specific work input W is the total work input per unit volume during the loading stage of that cycle. For each hysteresis loop, values of ΔW and W were calculated from true stress–strain data. Subscripts identify specific loops within a set of five that were all taken to a particular maximum strain. Thus ΔW_4 measures the area enclosed by the **fourth hysteresis loop** in a given set, while W_4 measures **all** of the area under the **fourth loading curve**, between zero stress at the beginning of that loading-unloading cycle, and $\sigma_{t,max}$. The fourth cycle in each set is of particular interest because at that stage hysteresis has almost reached a steady state; the fifth cycle is less suitable as a basis for comparison because maximum strains of 40 and 60 % are followed by large increases in $\varepsilon_{t,max}$.

The results of this analysis are shown in Fig. 4. To a good approximation, all of the points lie on a single straight line through the origin, thereby demonstrating that the same deformation mechanisms govern energy dissipation in all three polymers. To that extent, PE06, PE5 and PE9 exhibit the same behaviour. Fig. 4 shows that the main difference between them is that maximum values of W and ΔW are relatively high in PE5 and PE9, while they are relatively low in PE06. Two factors contribute to these differences: (a) at every stage of the test, residual strains at zero stress are lower after unloading in PE5 and PE9 than in PE06, so that larger strain increases are required to reach ε_{max}; (b) strain hardening effects are much more prominent in PE5 and PE9, so that peak stresses rise more rapidly in these materials. Despite the significantly higher initial yield stresses exhibited by PE06 because of its high crystallinity, it reaches slightly lower peak stresses than PE5 or PE9 during the final five cycles of the test, where $\varepsilon_{max} = 80$ %.

Optical microscopy was used to study the damage caused by cyclic loading. Small blocks of UHMWPE were cut for the microscope stage and the original moulded surfaces were carefully cleaned using an acetone

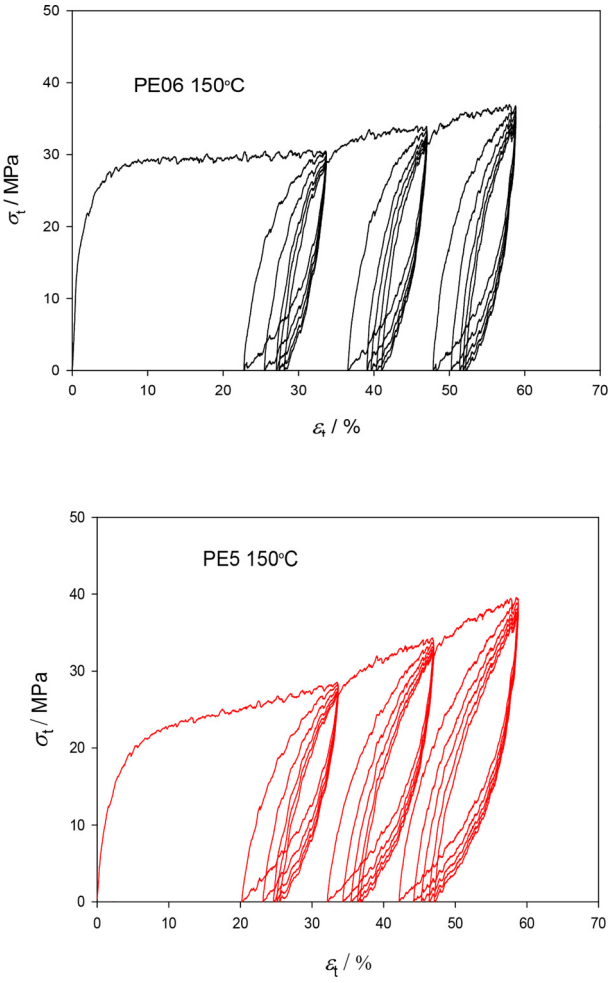

Fig. 3: Nominal stress–strain curves for PE06 and PE5 obtained in cyclic loading tensile tests at 19 °C and Hencky strain rate of 0.05 s^{-1}. Data from Buckley.

Table 3: Effects of moulding temperature and maximum true strain on relative residual true strain ε_r^* in PA06 – see Equation (3). Combined uncertainty $u_c = \pm 2.5$ %. Data from Buckley, (OU).

Maximum strain (%)			ε_r^*
	40	**60**	**80**
150 °C	0.68	0.78	0.81
165 °C	0.69	0.81	0.83
180 °C	0.69	0.80	0.82

solution. Nevertheless, the samples showed evidence of embedded debris, in addition to many scratches. To detect fusion defects and characterize anisotropy, sections were therefore prepared from the interiors of both freshly made and previously tested specimens. For examination under polarized light, each section was cut to a thickness of 50 μm, on planes perpendicular to the tensile bar's cross-section, then mounted between a glass slide and a cover slip in a liquid of matching refractive index.

In addition, environmental scanning electron microscopy (ESEM) was used to examine specimens both before and after testing. Prior to testing, there was little detectable evidence of surface void formation in any of the specimens. Following cyclic loading, both PE5 and PE9 appeared to be undamaged, but the PE06 specimens displayed a high density of surface voiding, as illustrated in Fig. 5.

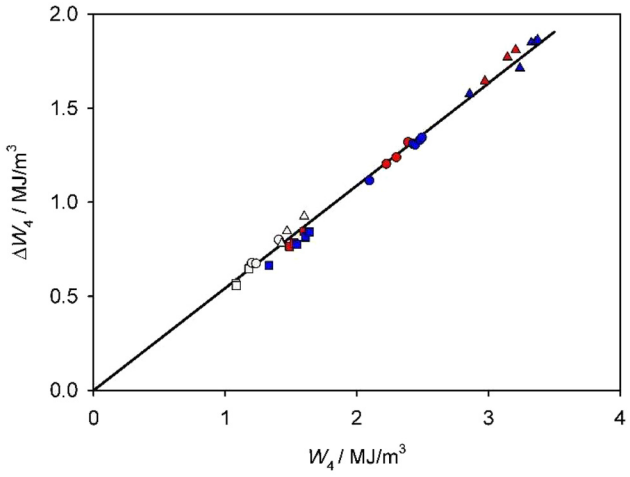

Fig. 4: Energy dissipated through hysteresis plotted against work input per unit volume in PE06 (open black symbols), PE5 (red symbols), and PE9 (blue symbols). Data obtained from fourth cycles in Fig. 3, at $\varepsilon_{max} = 40$ % (□), 60 % (○), and 80 % (Δ). Data from Buckley (OU).

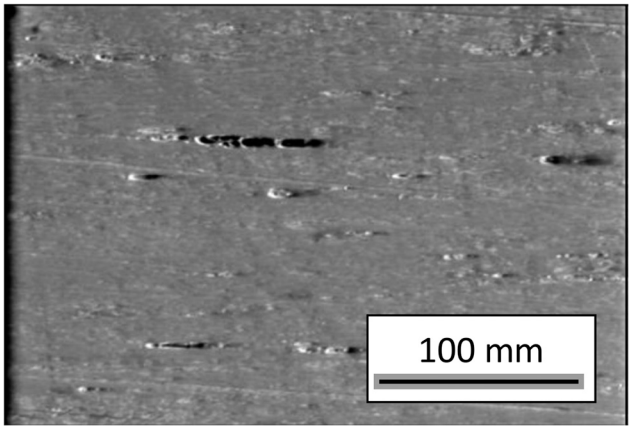

Fig. 5: Surface voids formed in a PE06 bar subjected to cyclic tensile loading in the horizontal direction, parallel to the voids. Data from Buckley (OU).

2.4 Small punch testing

Small punch tests (SPT) were carried out by Slouf at (23 ± 1) °C in accordance with the ASTM standard [3]. This test is designed specifically for testing UHMWPE, using specimens taken either from pristine manufactured implants or from implants retrieved from the human body [4]. The specimens are 0.5 mm thick and 6.4 mm in diameter. They are clamped around their circumference against the rim of a cylindrical die with an inner diameter of 3.81 mm. The punch is a cylindrical rod with a diameter of 2.54 mm and a hemispherical head, which is driven into the die at a velocity of 0.5 mm/min. In this study, at least five specimens of each material were tested. The standard requires that average and standard deviations of peak load, ultimate load, ultimate displacement, and work to failure be recorded.

The graphical results of small punch tests are presented in Fig. 6. They are broadly similar to those obtained in standard and cyclic tensile tests. The force-deflection curves for PE06 rise steeply to a peak, but the polymer then strain-softens quite rapidly. Curves for PE5 and PE9 have lower initial slopes and slightly lower peak forces. Beyond maximum load, the curves for both UHMWPE grades diverge by a small amount; strain softening takes place more slowly than in PE06 and is followed by strain hardening, which is more prominent in PE5 and PE9 because of their higher entanglement densities. The curves reach a minimum at a deflection of about 4 mm, which is a convenient point at which to compare the force data. This comparison demonstrates that the defining force $F_{4\,mm}$ at this deflection is only moderately sensitive to variations in the molecular weight of the selected polymers.

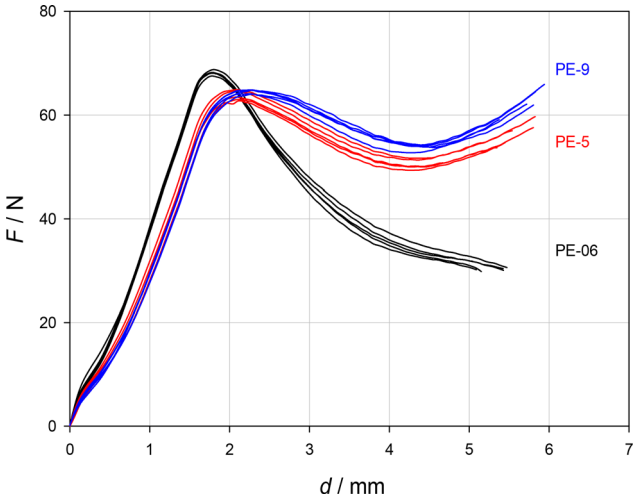

Fig. 6: Force-deflection curves from small punch tests on PE06, PE5, and PE9, each represented by five specimens. Data from Slouf (CZ).

2.5 Channel die compression

Galeski (PA) carried out channel die compression tests at a true strain rate of 0.067 s^{-1} in a 6 mm wide, 49.3 mm long rectangular channel. The compression tool was a closely fitting rectangular block. Specimens were 6.0 mm wide, 23.4 mm high, and 49.3 mm long. A full description of the test method is given in an article by Bartczak et al. [5]. Basically, the specimen extends along the length of the channel as it is compressed vertically. As illustrated in Fig. 7, the onset of plastic deformation is marked in all three grades of UHMWPE by a change in slope rather than a clear peak. It is therefore difficult to obtain accurate data on yield stresses from channel die compression tests. Best estimates of yield stresses in compression at 22 °C are 47 MPa for PE06 and 31 MPa for PE5 and PE9, with combined standard uncertainty $u_c = \pm 5\,\%$. These relatively high values are due to the pressure-dependence of plastic deformation, which is a characteristic feature of yielding in thermoplastics. As in the tensile tests, raising $\overline{M}_w$ from 5×10^6 to 9×10^6 had little effect on deformation behaviour, again indicating that increasing the entanglement density in the central regions of the powder particle 'grains' during compression moulding was not translated into higher resistance to deformation at room temperature. This observation supports the view that deformation in lightly entangled 'grain' boundaries made a disproportionately large contribution to yielding in compression.

2.6 Microhardness

Slouf carried out Vickers microhardness tests at 23 °C using a standard indenter [6]. Samples were first spattered with a 4 nm thick layer of platinum. Loads of 5, 10, and 50 g were then applied for 6 s, and the diagonal lengths d_i of the indentations were measured using an optical microscope. Plots of applied force F against d^2 were linear. In these tests, Vickers microhardness, $H_{V\mu}$, is given by:

$$H_{V\mu} = \frac{1.854 \times F}{d_i^2} \tag{4}$$

where the unit for microhardness is MPa, F is the force in N (Newton) and d_i is the indentation diameter in mm. Quoted results for $H_{V\mu}$ are based on the average of 10 separate measurements. The hardest material was PE06, with $H_{V\mu} = 57.6$ MPa. Hardness values for PE5 and PE9 were substantially lower, at 41.5 MPa, and 40.3 MPa, respectively, with $u_c = \pm 2\,\%$. Once again, the increase in $\overline{M}_W$ from 5×10^6 to 9×10^6 had little effect.

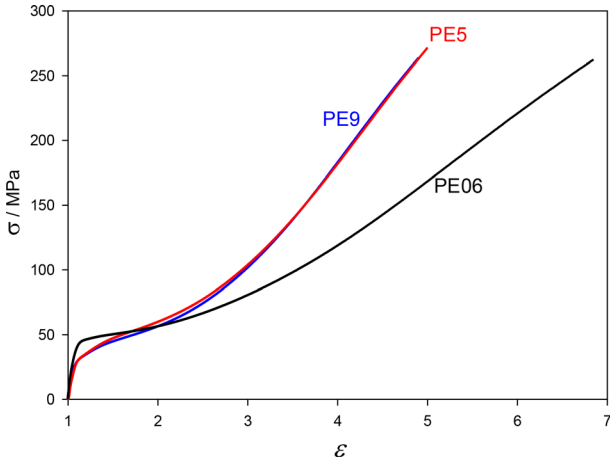

Fig. 7: Channel die compression curves showing compressive stress σ as a function of strain ε for PE06, PE5, and PE9 at 22 °C. Data from Galeski (PA).

2.7 Wear testing

Slouf used an OrthoPOD multidirectional pin-on-disc (POD) machine to measure wear rates, following the ASTM standard [7]. The metal discs were polished to a surface roughness *Ra* of 0.1, and the load on the UHMWPE pins was 4.0 MPa, which is approximately the contact stress in human joints.[2] The average pin-to-disc velocity was 6 cm/s. The total multidirectional path for each pin corresponded to 1 million cycles. Wear rate was calculated as the ratio of the mass lost by the sample to the mass lost by a control, which was a standard non-crosslinked Chirulen 1020 grade of UHMWPE. At least three repeat measurements were made on each material. The measured wear rates for PE06, PE5, and PE9 were 6.57, 0.86, and 1.52 respectively.

Wu used the Durham multidirectional pin-on-plate machine to perform bio-tribological wear tests on PE06, PE5, and PE9, following an ASTM standard with respect to patterns of motion, sliding speed, lubricant, and temperature [7]. The tests were carried out at 60 rpm, with 25 mm strokes at a sliding speed of 50 mm s^{-1}. A load of 40 N was applied vertically to each pin to give a contact stress of 2 MPa. The pins and plates were lubricated with 25 % (v/v) diluted bovine serum (Harlan Laboratories Limited, UK), which gave a protein content of approximately 17.5 g L^{-1}, with 0.2 % sodium azide (NaN_3) added to inhibit bacterial growth, along with 20 mM ethylene-diamine-tetra-acetic acid (EDTA) to prevent calcium deposition. The wear tests were conducted for up to 3 million cycles, stopping approximately every 0.25 million cycles to enable the pins and plates to be cleaned in accordance with the ISO cleaning/drying protocol [8], prepared for surface examination, and weighed using a Mettler AE 200 balance with an accuracy of 0.01 mg. Finally, before resuming the next 0.25 million cycles, fresh lubricant was applied to the clean surface.

The results are presented in Fig. 8. They show that PE06 had the highest rate of wear, at 0.153 μg m^{-1}, while the wear rates of PE5 and PE9 were lower and almost identical, at 0.08 μg m^{-1}. Under an optical microscope, a grain boundary pattern is clearly visible on the worn surface of the PE9 specimen shown in Fig. 9.

2.8 Fatigue crack growth testing

Wu studied fatigue crack propagation (FCP) in compact tension (CT) specimens under sinusoidal loading at 5 Hz, at 23 °C and 50 % relative humidity, in accordance with the ASTM standard [10]. Specimens 35 mm high and 36.5 mm wide were cut from 3 mm thick compression moulded plates provided by the UHMWPE manufacturer. Starter-crack slots were cut from one edge of each specimen to a length, a_0, of 13.5 mm along the

2 The arithmetic roughness *Ra* of a surface is obtained by making a large number of measurements, along a straight line, of deviations from a 'mean line' through the surface and taking the arithmetic average of these deviations. See ISO Standard [9].

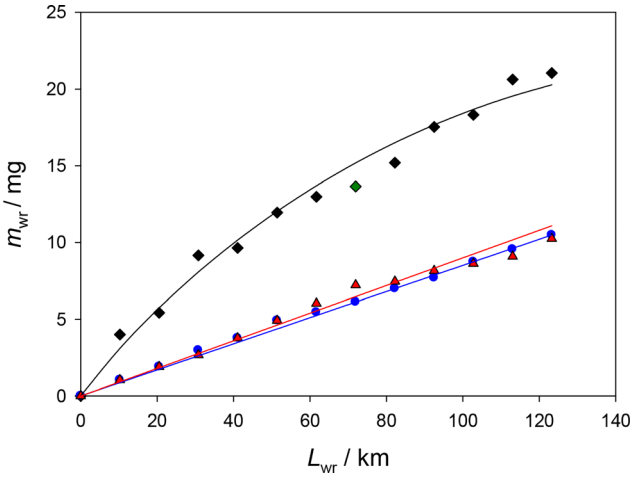

Fig. 8: Curves showing loss of mass m_{wr} with increasing length of travel L_{wr} in wear tests on PE06, PE5, and PE9. Wu (DU).

central plane, with faces 1 mm apart. Their tips were sharpened with a razor blade. Crack-opening cyclic tensile stresses were applied through pneumatic clamps attached across the upper and lower edges of the test specimen. The crack-tip stress intensity factor, K, was varied between a minimum, K_{min}, and a maximum, K_{max}, with R (the ratio K_{min}/K_{max}) set at 0.1. The magnitude of K in fracture mechanics is determined by the applied stress, σ, the crack length, a, and the geometry of the specimen, in accordance with the following equation:

$$K = Y\sigma(\pi a)^{0.5} \tag{5}$$

where Y is a numerical factor determined by the geometry of the test specimen [10].

Preliminary trials indicated that an initial crack-tip stress intensity amplitude ΔK of 1.75 MPa $m^{0.5}$ would initiate stable crack growth at a measurable rate. From an initial crack length a_o of 13.5 mm, a preferred nominal stress amplitude $\Delta\sigma$ of 4.47 MPa was identified. For each cycle, nominal applied stresses therefore ranged from a minimum of 0.497 MPa to a maximum of 4.97 MPa. The nominal stress is defined as the applied force, F, divided by the nominal cross-sectional area, BW, where B is thickness and W is width measured from the loading point. Earlier trials showed that temperature rises were negligible during fatigue crack propagation at 5 Hz in the 3 mm thick CT specimens.

With $\Delta\sigma$ and R held constant, ΔK increased with increasing crack length a. Specimens were marked with a felt pen at increments of 2 mm along the anticipated route of crack propagation, and tests were filmed using a Casio EXILIM EXZ720 digital camera with a resolution of 7.2 megapixels. Crack length a was recorded as a function of time t. The film was used to determine the time intervals required for visible increments in stable

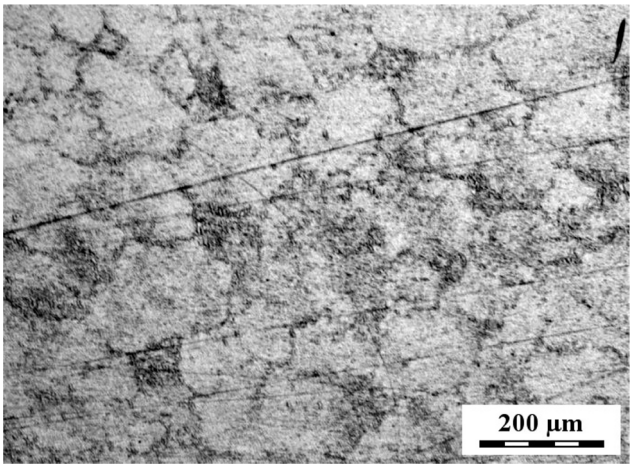

Fig. 9: Surface of PE9 plate after 3 million cycles of bio-tribological wear testing at 37 °C. Wu (DU).

crack growth. These data were used to calculate crack propagation rate, da/dN, as a function of ΔK, where N is the number of loading cycles.

Results from these tests are presented in Fig. 10, which covers the regions of stable crack growth in all three materials. In this region, propagation rates typically follow the Paris equation [11]:

$$\frac{da}{dN} = C(\Delta K)^m \tag{6}$$

where C and m are coefficients determined by the material's properties. Fatigue crack propagation can generally be divided into three stages. During the initial stage, there is little observable crack growth, but load cycling finally leads to a transition into the second stage, where stable crack propagation takes place at an increasing rate. In the third, terminal stage of the test, da/dN is large enough to make propagation unstable. Since stable crack growth behaviour is of the greatest interest in the present context, data from the initial and final stages of propagation are not included in Fig. 10. Both PE5 and PE9 clearly follow Equation (6), with m equal to 4.8 and 4.9 respectively. There are not enough data on PE06 to determine whether this grade of UHMWPE obeys Equation (5) in the stable growth region.

The most significant and unexpected result recorded in Fig. 10 is that resistance to fatigue crack propagation **decreased** with increasing molecular weight, so that the highest crack growth rates were exhibited by PE9. The obvious conclusions to be drawn from this observation are that (a) bonding between reactor powder particles was relatively weak, so that there was no gain in fracture resistance when $\overline{M}_w$ was raised from 5×10^6 to 9×10^6; and (b) fatigue tests are particularly effective at exposing this kind of weakness. The levels of entanglement at grain boundaries between adjacent powder particles appear to be relatively low in both UHMWPE grades, especially PE9. Environmental scanning electron microscopy showed that growth steps at intervals of approximately 2 µm were formed on the fracture surfaces of both PE5 and PE9 specimens towards the end of the fatigue test, but the fracture surface of PE06 was almost featureless – see Fig. 11.

A more extensive study led by Altstädt (UB) found that fatigue crack propagation behaviour in PE06, PE5, and PE9 was strongly dependent on the thickness of compact tension specimens. There was a certain amount of scattering in the data from 4 mm thick specimens, but da/dN generally increased with increasing ΔK, approximately in accordance with Equation (6). By contrast, crack propagation in almost all of the 10 mm thick specimens tested was extremely erratic, and in some cases impossible to initiate. Because of the significance and complexity of these results, they are presented and discussed separately in Part 4, the final report in this series).

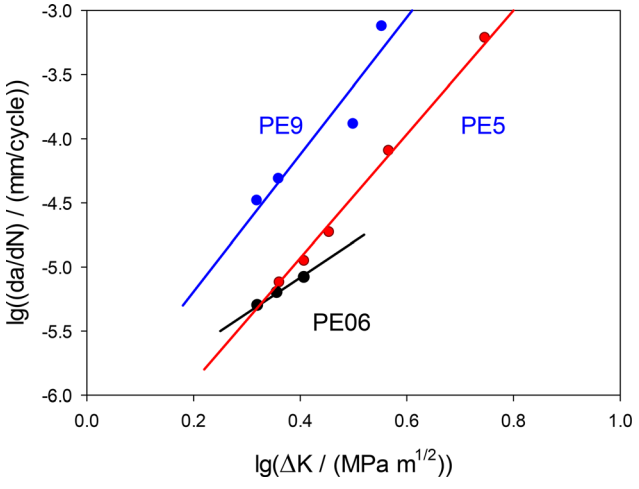

Fig. 10: Relationship between stress intensity amplitude ΔK and fatigue crack growth rate da/dN in 3 mm thick CT specimens. Data of Wu (DU).

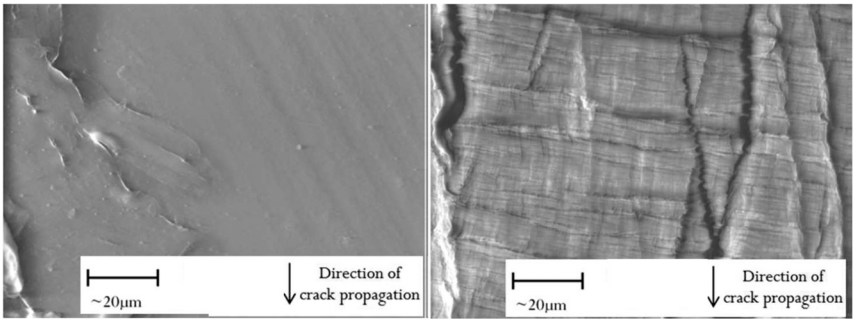

Fig. 11: Environmental scanning electron micrographs of fracture surfaces from compact tension specimens subjected to fatigue tests by Wu (UD); left PE06; right PE5.

3 Discussion

This study has shown that the mechanical properties of UHMWPE mouldings are dependent on molecular weight, but that increasing $\overline{M}_w$ from 0.6×10^6 to 5×10^6 had a much larger effect than increasing it from 5×10^6 to 9×10^6. The close similarity in properties between PE5 and PE9 is unexpected and needs explanation. At small strains, the deformation behaviour of all three grades of UHMWPE is largely dependent on their elastic moduli, which increase with crystallinity, χ_c. As freshly made powders, all three grades had crystallinities between 70 and 72 %, but compression moulding by the polymer manufacturer resulted in substantial decreases, down to 60 % in the case of PE06, and to 45 % in PE5 and PE9. Relatively long relaxation times prevented them from reaching 70 % when they were cooled in the mould. Because PE06 crystallizes more rapidly than PE5 and PE9, cooling left PE06 with the highest crystallinity, elastic modulus, and yield stress.

By contrast, annealing for 2 h at 235 °C raised χ_c to approximately 75 % in PE5 and PE9, and to about 90 % in PE06 – see Table 5 in Part 2 of this report. Prolonged heating can improve consolidation by enabling levels of entanglement to increase and the problems associated with fusion defects to be minimized, but these benefits have to be balanced against the inevitable damage resulting from thermal degradation and the increased costs of processing. For industrial manufacturers it is not a viable option. The minimum temperature for melt processing UHMWPE is 150 °C, and raising it above this level increases rates of chain scission. Consequently, melt-processing conditions are rarely (if ever) sufficient for compression mouldings to be extremely well consolidated. In the worst cases, substantial numbers of powder particles are in some areas simply not bonded to their immediate neighbours, and form Type 1 fusion defects. A more common problem is the formation of Type 2 defects, where entanglement has taken place, but levels are relatively low, so that samples tend to fail prematurely, especially under fluctuating loads. The challenge for manufacturers is to develop quantitative test methods that can determine precisely how well a melt-processed UHMWPE product is consolidated when perfect consolidation is extremely difficult, if not impossible. This issue is addressed at length in the fourth and final report in this series.

To quantify the extent of inter-particle diffusion expected during moulding of UHMWPE, Buckley, Wu, and Haughie have employed the 'reptation time', τ_d, which is the time taken by a molecule in the melt to escape from the enclosing 'tube' defined by its entanglements [12]. This would also be the time required to achieve complete entanglement across two contacting polymer surfaces, measured from the onset of wetting at time u,

Table 4: Mass fraction f of polymer contributing to interfacial bonding in mouldings made at three moulding temperatures, θ_{mould}, calculated using Equations (8)–(10), with $\Delta_{df}H^0 = 26$ kJ mol^{-1}, reference temperature $\theta^* = 180$ °C, and the reptation time $\tau_d = 10{,}400$ s at θ^*. Estimated combined standard uncertainty $u_c = \pm 10$ %.

θ_{mould}	f		
	150 °C	**165 °C**	**180 °C**
PE06	1.0	1.0	1.0
PE5	0.17	0.22	0.23
PE9	0.10	0.19	0.19

where 'wetting' means contact at the atomic level between the surfaces to be joined [13]. For a sample of polymer with a monodisperse distribution of molecular weights, reptation theory predicts:

$$\frac{\tau_{\mathrm{d}}}{\tau_{\mathrm{d}}^{*}} = \left(\frac{M}{M^{*}}\right)^{3.4} \tag{7}$$

where M is the molar mass of the sample, M^{*} is the molar mass of a reference polymer, and τ_{d}^{*} is the corresponding reptation time in the reference sample. Because of this relationship, the time taken for an interface to match the strength of the bulk material is, theoretically, strongly dependent on M.

A polymer chain of length L can be treated as being confined to an imaginary tube, the form of which is defined by the surrounding entangled chains. A chain forms fresh entanglements only after its ends have been liberated through reptation, leaving a smaller portion of length L' constrained within the tube. Consequently, f, the fraction of chain that is free to reinforce a bonding interface, is given by $(1 - L'/L)$. Using an equation developed by Doi and Edwards [14], Buckley et al. have shown that this is related to the reptation time τ_{d} by:

$$f = 1 - \sum_{k=1}^{\infty} \frac{8}{k^{2}\pi^{2}} \exp\left(-\frac{k^{2}\Delta\xi}{\tau_{\mathrm{d}}}\right) \tag{8}$$

where the summation is restricted to odd values of k, and

$$\Delta\xi = \int_{u}^{t_{s}} \frac{\mathrm{d}u}{a_{T}(u)} \tag{9}$$

is the elapsed effective time between inter-particle wetting (at a time u during heating) and solidification (at time t_{s} during cooling). The time-temperature shift factor, $a_{T}(u)$, is given by:

$$a_{T}(u) = \frac{\Delta_{\mathrm{df}}H^{0}}{\mathrm{R}}\left[\frac{1}{T(u)} - \frac{1}{T^{*}}\right] \tag{10}$$

where $\Delta_{\mathrm{df}}H^{0}$ is the activation enthalpy for self-diffusion in the melt and R *i*s the gas constant. In the present study, these equations were used to estimate the fraction f of polymer that become available for inter-particle diffusion, and hence the inter-particle entanglement, during the compression moulding process. The results are set out in Table 4. However, these results must be regarded as approximate. The three grades of UHMWPE provided for the present project are far from monodisperse. The molar masses quoted in this report are averages based on intrinsic viscosity measurements – see Part 1 of this series.

The low crystallinity of compression moulded PE5 and PE9 is due to greatly reduced rates of reptation in the melt state during cooling in the mould, relative to those in standard grades of linear PE with $\overline{M}_{\mathrm{W}}$ approximately 10^{5}. In UHMWPE, the chain segments close to chain ends are the most mobile, and are therefore incorporated preferentially into lamellae. Those located nearer the middle of the chain are less likely to contribute to crystallization and tend to form highly entangled networks within the amorphous regions [13]. At large plastic strains, crystallographic slip enables polymer chains to unfold and align themselves parallel to the direction of the applied load. The result is a plateau in the nominal stress–strain curve. However, because of the reduced crystallinity in true UHMWPE materials with $\overline{M}_{\mathrm{W}}$ above 10^{6}, this mechanism of deformation is exhausted relatively rapidly, so that strain hardening occurs at lower true strains in PE5 and PE9 than in PE06.

Raising the relative molar mass of linear polyethylene from 10^{5} to 5×10^{6} greatly increases its resistance to wear and enables it to function effectively in orthopaedic joint prostheses. However, the performance of these prostheses is adversely affected by the need to employ two separate processes in the manufacture of UHMWPE components. Ethylene monomer is first polymerized to form a fine powder, which is then consolidated by melt processing. Compression moulding and ram extrusion are widely used for this purpose. Electron microscopy and other experimental techniques show that products made in this way are often imperfect – see Fig. 9, for example. The outlines of the original powder particles are clearly visible in the micrograph. No such weak boundaries are formed in melt-processed high-density polyethylene (HDPE), where $\overline{M}_{\mathrm{W}}$ is generally below 10^{5} and reptation rates are much higher.

It is easy to make defect-free products in polymers with ultra-high $\overline{M}_W$ when the monomer can be converted directly into solid blocks, without requiring an intermediate consolidation step. The most obvious example is cast poly(methyl methacrylate) (PMMA), which is renowned for its transparency and is composed of extremely long chains, each of which forms a large number of entanglements during polymerization in the mould. Melt-processed UHMWPE falls far short of this ideal, especially at grain boundaries.

Figure 2 shows that all three grades of HMWPE exhibit broadly similar patterns of behaviour in standard tensile tests. At strains up to about 10 %, deformation is basically viscoelastic rather than plastic, and crystallinity is the dominant factor controlling properties. The stress therefore increases most steeply in PE06, which is substantially more crystalline than PE5 and PE9. Beyond the yield point, plasticity begins to dominate and the direct influence of molecular weight becomes more apparent; at nominal strains up to 200 %, PE06 exhibits pronounced strain softening, whereas PE5 and PE9 strain harden. However, there is no consistent trend with moulding temperature. When the data are used to produce true stress-true strain curves, all three grades of UHMWPE can be seen to strain harden from the yield point onwards, but the rate of hardening is much lower in PE06. The difference can be attributed to a large contribution from long-range stress relaxation in this polymer, as opposed to localised, reversible, rubber-like stretching of the entanglement network in the two UHMWPE grades.

The behaviour of PE06, PE5, and PE9 in cyclic tensile loading tests can be modelled by treating each specimen as a two-phase structure, with the soft amorphous fraction in series with the harder crystalline phase. The differences in cyclic response and deformation between the three grades can be attributed to differences in entanglement density in the amorphous phase. Furthermore, the results suggest that loading to higher strain levels causes lamellae to break up, thereby increasing the amorphous fraction, whereas cycling between fixed strain levels results in re-crystallization. Accumulated plastic deformation during cyclic loading of UHMWPE is one of the factors affecting wear in knee joint prostheses, and can ultimately lead to fracture. One widely used solution to this problem is to cross-link the polymer. However, the resulting increase in wear resistance has to be balanced against reductions in both ductility and fracture resistance.

The curves obtained from small punch tests are similar to the stress–strain curves from tensile tests. Because of its higher crystallinity, the applied forces initially rise most rapidly in PE06, leading to a higher peak at the onset of yielding, followed by strain softening. By contrast, yielding and strain softening in PE5 and PE9 are followed by strain hardening.

Channel die compression tests provide valuable information about the pressure-dependence of yielding in polymers, which is represented by a modified version of the von Mises yield criterion [15, 16]:

$$\sigma_e = \left[\frac{(\sigma_1 - \sigma_2)^2 + (\sigma_2 - \sigma_3)^2 + (\sigma_3 - \sigma_2)^2}{2}\right]^{0.5} = \sigma_{Y0} - C\sigma_m \tag{11}$$

where σ_e is the effective stress, which drives yielding, σ_m is the mean stress (negative pressure), which induces small elastic volume changes in the polymer, σ_{Y0} is the characteristic yield stress of the polymer, which is dependent on temperature and strain rate but unaffected by changes in σ_e and σ_m, and C is a simple numerical factor. In metals, for which the von Mises criterion was originally developed, $C = 0$.

A consistent feature of the mechanical test data obtained during this project is that there is little or no difference in stress–strain behaviour between PE5 and PE9. In theory, entanglement density should be significantly higher in PE9, because it has longer chains, and that should be reflected in its mechanical properties. A comparison of data from PE06 and PE5 provides a good example of what would be expected, and there is a marked difference between PE5 and PE9 in tensile tests at 150 °C – see Part 1 of this series. The simplest explanation for the observation that the differences between PE5 and PE9 are quite small at room temperature is that entanglement densities at grain boundaries in PE5 and PE9 were well below the levels theoretically obtainable in fully-consolidated mouldings and that the increase in entanglement obtained in these boundary regions by raising $\overline{M}_W$ to 9×10^6 was relatively small. Raising the temperature to 150 °C, above the melting point of polyethylene, enables entanglements to form before tensile stresses are applied.

Pawlak, Galeski, and Rozanski have published a comprehensive review of the factors affecting cavitation in semi-crystalline polymers, which notes that voids form in the (elastomeric) amorphous phase of polyethylene in response to an imposed dilatational stress [17]. The volume fraction and properties of the crystalline phase are therefore important, because they determine whether the polymer yields before the onset of cavitation. Studies on HDPE, which has a $\overline{M}_W$ of about 10^5, show that annealing increases crystallinity and lamellar thickness, so that the volume fraction of amorphous phase is reduced and the density of entanglements in that phase is increased. Consequently, the tensile yield stress is raised and the amorphous phase becomes more susceptible to cavitation [18]. Methods used to detect void formation include SAXS, electron microscopy, visual observation of stress-whitening, optical microscopy, and measurements of volume strain. Factors that determine whether cavitation will take place in an HDPE sample include strain rate, temperature, and the ratio of the mean stress, σ_m, to the deviatoric stress σ_e. Under uniaxial tension, $\sigma_m/\sigma_e = 1/3$, and the material might or might not cavitate in a standard test at 23 °C, depending on its crystallinity and the other factors listed above. Substantially increasing the ratio σ_m/σ_e will inevitably lead to widespread void formation or fracture.

In the present study, data from pin-on-plate and pin-on-disc tests confirm that the wear resistance of UHMWPE is improved substantially by raising $\overline{M}_W$ from 0.6×10^6 to 5×10^6 or more. One factor responsible for this improvement is the increase in post-yield drawing stress. Similar effects are seen in micro-hardness tests, where there is an increased resistance to indentation. However, the numerical data from standard tests provide no direct information about the mechanisms responsible for wear in UHMWPE. In that context, micrographs of wear surfaces are of more interest. They show that wear in both PE5 and PE9 is most intense near 'grain boundaries.' Furrows outlining grains with diameters of about 100 μm are clearly visible in Fig. 9. On the basis of these observations, the possibility of including microscopy of wear surfaces in QA and QC procedures should be considered. However, it would be effective only if the method can be shown to differentiate reliably between satisfactory and sub-standard mouldings. Further work is required before any firm recommendation can be made.

It is important to note that high wear resistance, as measured in standard tests, does not guarantee satisfactory performance in hip and knee prostheses. The main problem is not the loss of material, but the body's response to UHMWPE wear debris, which in some cases can be catastrophic. Our blood vessels contain *macrophage* cells, which detect microscopic foreign bodies, such as bacteria or fragments of natural bone, and send white blood corpuscles called phagocytes to destroy them. In particular, *primary human peripheral blood mononuclear phagocytes* are programmed to produce proteins called *osteolytic cytokines*, which break down natural bone fragments. The quantity of cytokines formed in this way is a measure of **biological activity** $\beta(r)$. If the initial response to wear particles does not solve the problem, the body sends more phagocytes to the affected area. Consequently, when phagocytes fail to dispose of UHMWPE wear debris, they increase in number and then tend to attack the bone nearby, causing pain and loosening the prosthetic implant, so that replacement surgery becomes necessary.

Matthews and co-workers have studied the effects of UHMWPE wear particles on $\beta(r)$ by blending particles of various sizes with the relevant phagocytes, culturing the blends for 24 h, and measuring the levels of the cytokines formed during this period [19]. They found that the phagocyte cells remained fully viable after the tests were completed, so that the results were not affected by changes in the availability of cytokines. There is no set scale for $\beta(r)$ in Fig. 12. The activity is taken as 1.0 for particles between 0.1 and 1.0 μm in diameter. It has progressively lower values for particles with larger diameters. The challenge for manufacturers of UHMWPE is to reduce the formation of very small wear particles, so that unwanted and detrimental biological activity is substantially reduced.

In recent years, investigators have been able to develop improved, more quantitative approaches to the design of artificial joints, in which wear tests are based on hip joint simulators, where UHMWPE and a CoCrMo alloy form the two bearing surfaces. Scanning electron microscopy is used to obtain images of the resulting wear debris particles, and advanced mathematical methods are used to characterize that debris [20, 21]. One recent study by Bian and co-workers goes a step further, by applying these techniques to a novel grade of UHMWPE, which they call ultra-low-wear polyethylene [22]. As this polymer also forms wear debris particles with unusual shapes, they claim that it could enable artificial joints to operate successfully for a lifetime.

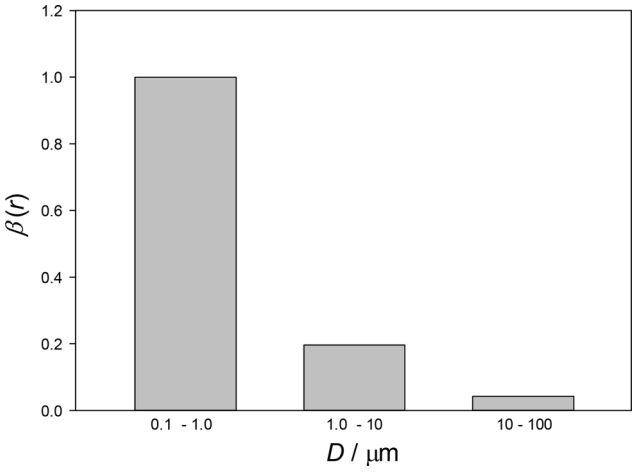

Fig. 12: Effects of wear particle size *D* on biological activity *β(r)* measured *in vivo* [19].

4 Membership of sponsoring bodies

Membership of the Subcommittee on Structures and Properties of Commercial Polymers during the preparation of these Reports was: **Chair**: Yongfen Men (China); **Secretary**: Yujing Tang (China); **Members**: Volker Altstädt (Germany); Lijia Am (China); Oliver Arnolds (USA); Dietmar W. Auhl (Netherlands); Paul Buckley (UK); Clive B. Bucknall (UK); Peng Chen (China); lldoo Chung (S. Korea); Dirk J. Dijkstra (Germany); Andrzej Galeski (Poland); Christoph Gögelein (Germany); Chang-Sik Ha (S. Korea); Mijeong Han (S. Korea); Ulrich Handge (Germany); Jiasong He (China); Sven Henning (Germany); Jun-ichi Horinaka (Japan); Wenbing Hu (China); Dae Woo Ihm (S. Korea); Tadashi Inoue (Japan); Takaharu Isaki (Japan); Akihiro Izuka (Japan); Xiangling Ji (China); Michail Kalloudis (UK); Dukjoon Kim (S. Korea); Jin Kon Kim (S. Korea); Sung Chul Kim (S. Korea); Seong Hun Kim (S. Korea); D. Su. Lee (S. Korea); Won-Ki Lee (S. Korea); Jae Heung Lee (S. Korea); Soonho Lim (S. Korea); Chengyang Liu (China); Shu-ichi Maeda (Japan); Mario Malinconico (Italy); Goerg Michler (Germany); Koh-Hei Nitta (Japan); Ewa Piorkowska-Galeska (Poland); Jinliang Qiao (China); Artur Rozanski (Poland); Dong Gi Seong (S. Korea); Tongfei Shi (China); Hongwei Shi (China); Sampat Singh Bhatti (Germany); Miroslav Slouf (Czech Republic); Zhaohui Su (China); Toshikazu Takigawa (Japan); Katsuhisa Tokumitsu (Japan); Kenji Urayama (Japan); Tatana Vackova (Czech Republic); Silvie Vervoort (Netherlands); Iakovos Vittorias (Germany); Yanwei Wang (Kazakhstan); Jun Jie Wu (UK); Donghua Xu (China); Masayuki Yamaguchi (Japan); Myung Han Yoon (S. Korea); Wentao Zhai (China); Wim Zoetelief (Netherlands).

Membership of the IUPAC Polymer Division Committee for the period 2020–2021 is as follows: **President**: C. K. Luscombe (USA); Past President: G. T. Russell (New Zealand); **Vice President**: I. Lacík (Slovakia); **Secretary**: P. D. Topham (UK); **Titular Members**: M. C. H. Chan (Malaysia); C. Fellows (Australia); R. C. Hiorns (France); R. Hutchinson (Canada); D. S. Lee (Korea); John B. Matson (USA); **Associate Members**: S. Beuermann (Germany); G. Moad (Australia); Marloes Peeters (UK); C. dos Santos (Brazil); P. Théato (Germany); M. G. Walter (USA); National Representatives: Ana Aguiar-Ricardo (Portugal); Jiasong He (China); C.-S. Hsu (Taiwan); Melina T. Kalagasidis Krušić (Serbia); P. Mallon (South Africa); O. Philippova (Russia); Guido Raos (Italy); M. Sawamoto (Japan); A. Sturcova (Czech Republic); Jan van Hest (Netherlands).

Acknowledgments: The authors thank the students and research staff who contributed to this project: Christopher Archer (Oxford), Alexander Brückner (Bayreuth), Richard Dusin (Lanxess) D. Di Francesco (Durham), Przemyslaw Sowinski (Lodz), Qian Qiang Wang (Durham), Kinga Zapala (Lodz), Rico Zeiler (Bayreuth).

Research funding: Project 2010-019-1-400 was supported by a grant from IUPAC. Funder ID: 10.13039/100006987.

References

[1] ASTM Standard D638-10. *Tensile Test Methods for Plastics*. ASTM International, West Conshohocken, PA (2010), www.astm.org.
[2] ISO Standard 527-1. *Tensile Test Methods for Plastics* (2012).
[3] ASTM Standard F2183-02. *Standard Test Method for Small Punch Testing of Ultrahigh Molecular Weight Polyethylene in Surgical Implants*. ASTM International, West Conshohocken, PA (2002), www.astm.org.
[4] F. Lednicky, M. Slouf, J. Kratochvil, J. Baldrian, D. J. Novotna. *Macromol. Sci. B Phys.* **46**, 521–531 (2007).
[5] Z. Bartczak, P. F. M. Beris, K. Wasilewski, A. Galeski, P. J. Lemstra. *J. Appl. Polym. Sci.* **125**, 4155 (2012).
[6] ISO Standard 14577. *Standardized Nanoindentation*.
[7] ASTM Standard F732. *Test Method for Wear Testing of Polymeric Materials for Use in Total Joint Prostheses*. ASTM International, West Conshohocken, PA, www.astm.org.
[8] ISO Standard 14243. *Implants for Surgery- Wear Testing Knee-Joint Prostheses - Part 1 Loading and Displacement Parameters for Wear Testing Machines With Load Control and Corresponding Environmental Conditions for Test*.
[9] ISO Standard 4287. *Geometric Product Specifications (GPS) – Terms, Definitions and Surface Texture Parameters*.
[10] ASTM Standard E647-5. *Standard Test Method for Measurement of Fatigue Crack Growth Rates*. ASTM International, West Conshohocken, PA (2005), www.astm.org.
[11] T. L. Anderson. *Fracture Mechanics: Fundamentals and Applications*. 4th ed. CRC Press, Baton Rouge, Florida, USA (2017).
[12] C. P. Buckley, J. J. Wu, D. W. Haughie. *Biomaterials* **27**, 3178 (2006).
[13] Y. Boontongkong, R. E. Cohen, M. Spector, A. Bellare. *Polymer* **39**, 6391 (1998).
[14] M. Doi, S. F. Edwards. *The Theory of Polymer Dynamics*. Oxford University Press, Oxford, UK (1988).
[15] L. Holliday, J. Mann, G. A. Pogany, H. L. D. Pugh, D. A. Gunn. *Nature* **202**, 381 (1964).
[16] R. N. Haward, R. J. Young. *The Physics of Glassy Polymers*. 2nd ed. Chapman & Hall, London (1997).
[17] A. Pawlak, A. Galeski, A. Rozanski. *Prog. Polym. Sci.* **39**, 921 (2014).
[18] A. Pawlak, A. Galeski. *Polymer* **51**, 5771 (2010).
[19] J. B. Matthews, A. A. Besong, T. R. Green, M. H. Stone, B. M. Wroblewski, J. Fisher, E. Ingham. *J. Biomed. Mater. Res.* **52**, 296 (2000).
[20] D. G. Eckold, K. D. Dearn, D. E. T. Shepherd. *Comput. Methods Biomech. Biomed. Eng. Imaging Vis.* **6**, 226 (2018).
[21] D. M. Zhang, H. T. Liu, J. Wang, C. Sheng, Z. Li. *J. Nanosci. Nanotechnol.* **18**, 6805 (2018).
[22] Y. Y. Bian, L. Zhou, G. Zhou, Z. M. Jin, Z. K. Hua, X. S. Wang. *J. Mech. Behav. Biomed. Mater.* **82**, 87 (2018).